

THE PENNSYLVANIA STATE UNIVERSITY  
SCHREYER HONORS COLLEGE

DEPARTMENT OF MECHANICAL ENGINEERING

INVESTIGATION OF TRIBOELECTRIC CHARGE GENERATION DURING ADHESIVE  
PEELING

SARAH CHEKAN  
SPRING 2024

A thesis  
submitted in partial fulfillment  
of the requirements  
for baccalaureate degrees  
in Mechanical Engineering  
with honors in Mechanical Engineering

Reviewed and approved\* by the following:

Zoubeida Ounaies  
Professor of Mechanical Engineering  
Thesis Supervisor

Xiaoyue Zhao  
Materials Research Institute Postdoctoral Scholar  
Thesis Co-Supervisor

Daniel Cortes  
Professor of Mechanical Engineering  
Honors Adviser

\*Signatures are on file in the Schreyer Honors College.

# Abstract

Triboelectricity is a commonly experienced natural phenomenon, yet its underlying mechanisms remain ambiguous amongst the scientific community. The inherently complex nature of triboelectricity necessitates an interdisciplinary approach to its study, integrating mechanics, material science, physics, and chemistry. Gaining a better understanding of the underlying mechanisms of triboelectricity and maximizing the predictability of charge generation will lead to the development of triboelectric nanogenerators (TENG). TENGs offer a sustainable method of powering integrated system sensors, replacing the traditional battery or capacitor that needs to be recharged or replaced after a limited time. The goal of this thesis is to investigate the mechanics of triboelectric charge generation, specifically the relationship between the separation speed of two surfaces and the resulting charge magnitude. Through imposing the well-studied and relatively simple mechanics of peeling onto a triboelectric system and through automating the peeling process to maximize the repeatability of experimental trials, the relationship between separation speed and charge generation is explored. Four experimental methods are developed to achieve the research goals, including manual and automatic procedures for both the measurement of the peel angle and generated charge. The peel angle, a key variable in all fundamental peeling equations and traditional peel test configurations, is measured through recording the unrolling of a spool of Scotch tape via manual and automatic means and measuring key angles throughout the trial in video post processing. Charge measurements are collected by an electrometer as a Scotch tape-copper tape composite is unpeeled manually and automatically. These experimental set ups are successfully modeled on traditional peel test configurations, accomplishing the objective of imposing simple mechanics onto a triboelectric system. While the focus on peeling mechanics simplified the system, the inherent complexity of adhesive properties materializes in the experimental results, specifically the adhesive stick-slip regime, adding a different layer of complexity. Experimental methods for both angle and charge that employed slower peel speeds and uniform test specimen proved to yield the most consistent and repeatable results; they were even superior to automating the process. Through developing more consistent methods of fabricating test specimen, integrating a motor controller into the system, investigating the adhesive properties of the test specimen, and integrating purposeful instabilities into the peeling process, more progress can be made in the exploration of the relationship between separation speed and triboelectric charge generation in the future.

# Table of Contents

<b>List of Figures</b>	<b>iii</b>
<b>Acknowledgements</b>	<b>iv</b>
<b>1 Introduction</b>	<b>1</b>
1.1 Background and Motivation . . . . .	1
1.2 Problem Statement . . . . .	3
1.3 Literature Discussion . . . . .	3
1.3.1 Peel Test Basics . . . . .	3
1.3.2 Peel Test Applications . . . . .	5
<b>2 Methods and Materials</b>	<b>7</b>
2.1 Angle Measurement . . . . .	8
2.1.1 Manual Angle Measurement Procedure . . . . .	8
2.1.2 Automatic Angle Measurement Procedure . . . . .	10
2.2 Charge Measurement . . . . .	13
2.2.1 Manual Charge Measurement Procedure . . . . .	13
2.2.2 Automatic Charge Measurement Procedure . . . . .	14
<b>3 Results and Discussion</b>	<b>15</b>
3.1 Angle Measurements . . . . .	15
3.1.1 Manual Angle Measurements . . . . .	15
3.1.2 Automatic Angle Measurements . . . . .	18
3.2 Charge Measurements . . . . .	19
3.2.1 Manual Charge Measurements . . . . .	19
3.2.2 Automatic Charge Measurements . . . . .	20
<b>4 Conclusions and Future Work</b>	<b>22</b>
4.1 Conclusions . . . . .	22
4.2 Future Work . . . . .	23
<b>Bibliography</b>	<b>25</b>
<b>Appendices</b>	<b>26</b>
A SolidWorks Sketches . . . . .	26
B Breadboard Configuration . . . . .	31
C Arduino Code . . . . .	32

# List of Figures

1.1	Illustration of TENG configurations . . . . .	2
1.2	Summary of types of peel test configurations . . . . .	4
1.3	Traditional peel test geometry . . . . .	5
1.4	X-ray generation set up . . . . .	5
1.5	Experimental configuration and results from study by Zhang et al. . . . .	6
2.1	Outline of experimental procedures . . . . .	8
2.2	Manual angle measurement procedure experimental set up . . . . .	9
2.3	Geometry relating measured experimental angle, traditional peel angle, and physical set up geometry of manual angle measurement procedure . . . . .	10
2.4	The top view and front view of the automatic angle measurement procedure experimental set up. . . . .	11
2.5	Geometry relating measured experimental angles to traditional peel angle for automatic angle measurement procedure. . . . .	13
2.6	Manual charge measurement procedure experimental set up . . . . .	14
3.1	Peel angle measurements for four trials for manual angle measurement procedure with a 0.555 kg drop mass. . . . .	16
3.2	Peel angle measurements for four trials for manual angle measurement procedure with a 1.500 kg drop mass. . . . .	17
3.3	Comparison of peel angle for 0.555 kg and 1.500 kg trials . . . . .	18
3.4	Peel angle measurements from automatic angle measurement procedure with a motor speed of 150 rpm and 250 rpm as well as a comparison between the two speeds. . . . .	19
3.5	Charge measurements from manual charge measurement procedure for “slow” trials and “fast” trials as well as a comparison between speeds . . . . .	20
3.6	Automatic charge measurements . . . . .	21
A.1	Tape mount dimensions . . . . .	26
A.2	Rotating core dimensions . . . . .	27
A.3	Tape spool dimensions . . . . .	28
A.4	Supported mount half dimensions . . . . .	29
A.5	Unsupported mount half dimensions . . . . .	29
A.6	Motor mount dimensions . . . . .	30
A.7	Motor spool dimensions . . . . .	30
B.1	Breadboard configuration to interface motor and Arduino . . . . .	31

# Acknowledgements

First, I would like to thank my thesis supervisor, Dr. Zoubeida Ounaies. Through giving me the opportunity to participate in the iPRISM Summer Research Program, integrating me into EMCLab upon returning from Freiburg to continue my work, and supporting me throughout the entire thesis process, this uniquely rewarding thesis experience would not have been possible without your expertise, guidance, and efforts on my behalf. I have learned so much about the world of research through participation in the iPRISM program and joining EMCLab, gaining valuable skills that I will carry with me throughout my future academic pursuits.

Thank you to Dr. Cortes, my honors adviser, for your time and support over the past few years as I have navigated the thesis process and grappled with my various post-graduation plans. I greatly value your thoughtful insights and advice.

I would like to thank Dr. Lars Pastewka and Dr. Viacheslav Slesarenko from the University of Freiburg for their support and guidance throughout my eight weeks in Freiburg, Germany over the summer of 2023. Your enthusiasm for this project is contagious, and I greatly appreciate having had the opportunity to collaborate with you both on this project.

I would also like to thank Dr. Xiaoyue Zhao for your continuous support over the past two semesters. I appreciate your patience and guidance as you welcomed me to EMCLab and guided me through this project. Thank you to Adam Racz and Dr. Michael Somr for your unwavering dedication to and support of this project over the summer of 2023, even when our experiments became the talk of the FIT building.

Thank you to EMCLab for providing valuable input and insights during our group meetings. I would also like to acknowledge the Mechatronics course ME 454 at Penn State for providing the rotational motor, breadboard, and Arduino configuration that is used throughout this thesis.

Finally, I would like to thank my friends and family. Thank you for believing in me and for offering much needed words of encouragement. This would not have been possible without your unwavering support.

# Chapter 1

## Introduction

### 1.1 Background and Motivation

Since the time of the Ancient Greeks, scientists have been fascinated by the concept of triboelectricity. To the average person, triboelectricity appears simple. Children understand a balloon will stick to the wall after rubbing it in their hair or sliding in socks across a carpet will allow them to “shock” their friend. However, further scientific investigation uncovers the innate complexity of this phenomenon.

Triboelectricity is the generation of charge due to the contact and separation of two materials [1]. Upon the separation of two materials after contact, the respective surfaces become oppositely charged. While this is a known occurrence, the underlying mechanisms behind this surface electrification remain ambiguous. Theories explaining potential charge sources include the creation and breakage of chemical bonds [1], which necessitates the integration of mechanochemistry into the study of triboelectricity. The true charge transferring mechanism is also unknown, with theories including the exchange of charged material fragments dependent on the relative surface roughness of the participating materials [2]. These ambiguities are compounded by the fact that the magnitude of triboelectric charge generated is difficult to predict outside of very controlled experimental environments. In addition, the surface morphology of the interacting surfaces can vary between samples, which in turn may influence the magnitude of charge generated for a given experimental trial. More difficulties in analysis arise since motion is required for triboelectric events to occur, resulting in the need for the study of this phenomenon to take place in a dynamic state rather than a static one. As a result of these factors, the exploration of triboelectricity becomes a multidisciplinary effort, requiring the incorporation of mechanics, materials science, physics, and chemistry.

Overcoming the challenges in investigating triboelectricity and gaining a better understanding of the mechanisms behind this phenomenon can lead to applications in a wide range of fields, specifically in the development of triboelectric nanogenerators. Triboelectric nanogenerators (TENG)

are devices that convert mechanical energy into electrical energy based on the generation of triboelectric charge due to the separation of surfaces [3]. There are several different configurations of TENG, summarized in Figure 1, all of which have the same fundamental set up. Each TENG has multiple layers consisting of electrodes and different dielectric materials [4]. These layers moving in relation to one another generate triboelectric charge, producing an electrical output from this mechanical motion. The continued development of TENG is particularly attractive given the fact that they offer a sustainable alternative to the batteries and capacitors that are typically used to power system sensors [3]. TENGs utilize an energy source inherent to the environment in which they are installed (mechanical motion), significantly reducing the need for replacement or recharging as needed with batteries and capacitors. This makes TENG ideal for powering sensors in locations that are hard to access. However, optimal use of TENG depends on the thorough understanding of the magnitude of triboelectric charge that is generated due to the mechanical motion between the TENG layers, which is a complex and multifaceted topic.

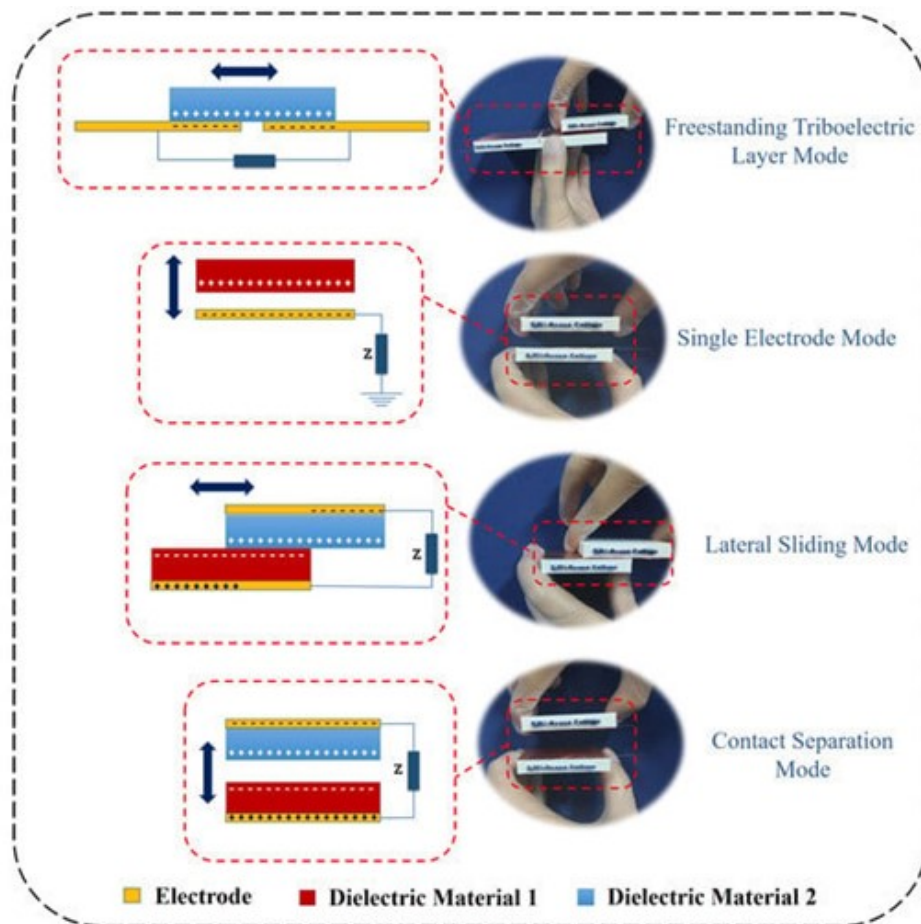


Figure 1.1: Illustration of TENG configurations [4].

## 1.2 Problem Statement

Given the ambiguities surrounding the mechanics that drive the generation of triboelectric charge, the goal of this thesis is to relate surface separation speed to the generation of triboelectric charge. Surface separation speed is selected as the parameter to relate to charge in order to leverage the research previously done in mechanics, particularly in mechanics of adhesives and peeling. Peeling mechanics has been thoroughly studied and consequently has a strong set of fundamental mechanical equations which relate parameters such as peel force, peel angle, material properties, and specimen geometry. Through relating the generation of triboelectric charge to the motion of peeling, the relationship between general mechanics and charge generation is then developed.

The first objective of this research is to impose mechanics with well-established mechanical equations onto a triboelectric system through employing peeling. There currently does not exist substantial understanding of the overall mechanics behind triboelectricity, so pairing this phenomenon with controllable motion that is relatively straightforward to analyze will allow for the exploration of the relationship between mechanical motion and the generation of charge. The motion of peeling is well studied [6] and has a set of well-established mechanical equations where peel angle, specimen geometry, and specimen material properties can be used to calculate the force necessary to peel an adhesive. Through associating the generation of charge with the motion of peeling, variables controlled by the peeling equations, such as peel force and peel angle, can potentially be associated with the generation of charge.

The second objective is to maximize consistency and repeatability of trials through automating the peeling motion. Triboelectric charge generation is known for its unpredictability and lack of consistency. Typically, automatic experimental procedures are the most controlled and repeatable through their goal to eliminate human interaction with the system as much as possible. The measurement of each parameter will initially utilize a manually driven experimental set up and eventually transition to an automatic process to improve repeatability. This automated process is materialized in the form of a rotational motor unpeeling a spool of tape coupled with an electrometer and high-speed camera to collect simultaneous charge and peel angle measurements.

## 1.3 Literature Discussion

In this section, general information on the peel test is discussed along with previous applications of peeling in the literature and the overall relevance to the research goals in this thesis.

### 1.3.1 Peel Test Basics

In a traditional peel test, a flexible adhesive is peeled from a rigid substrate. The angle from which the adhesive is peeled can vary, and the applied peel force can also differ between tests. From testing the performance of packaging to exploring the fracture mechanics of composite materials, the peel test can offer insights into key material properties [5]. The wide range of applications of this test yields a wide variety of experimental configurations, each focusing on a different type of material or material property. A summary of general peel test set ups is illustrated in Figure 1.2.





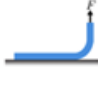

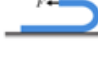






Summary of peel designations and relevant standards						
Schematic	Test	Representative Standards	Schematic	Test	Representative Standards	
	0° peel	ASTM D3654: static shear adhesion of PSA tapes (creep rupture) ASTM D6463: time to failure under sustained shear PSTC-7: "holding power" of PSA tapes PSTC-17: shear adhesion failure temperature (SAFT)		Loop tack	ASTM D6195: adhesive loop tack strength testing	
	90° peel	ASTM D6862: peel resistance of adhesives ISO 8510-1: flexible-bonded-to-rigid assemblies ISO 813: rubber adhesion to rigid substrate ASTM D6252: pressure-sensitive label stocks BS-EN-1895: paper and board, packaging, and disposable sanitary products ASTM B533: "peel strength" of metal electroplated plastics ASTM D3330 (method F): pressure-sensitive tape		Trouser tear	ASTM-D624: standard test method for tear strength of conventional vulcanized rubber and thermoplastic elastomers	
	180° peel	ASTM D903: peel of stripping strength of adhesive bonds ISO 8510-2: flexible to rigid bonded assemblies ASTM D3330 (method A): pressure-sensitive tape ASTM C794: adhesion-in-peel of elastomeric joint sealants		German wheel	DIN 53357: testing of plastic sheets; Adhesion test	
	T-peel	ASTM D1876: peel resistance of adhesives ISO 11339: flexible-to-flexible bonded assemblies ASTM D2918: durability of adhesive joints stressed in peel BS-EN-1895: paper and board, packaging, and disposable sanitary products ASTM F2256: tissue adhesive characterization		Climbing drum	ASTM D1781: for flexible to rigid adhesion ASTM D429: rubber to metal adhesion ASTM D2558: shoe sole adhesion	
	Mandrel peel	Not a standardized peel test		Floating roller	ASTM D3167: peel resistance of (structural) adhesive bonds ISO 4578: peel resistance of (structural) adhesive bonds ISO 14676: wet-peel for aluminum surface treatments ISO 22631: Peel of floor and wall covering adhesives	
				Impact wedge	ISO-11343: impact wedge peel (IWP) method	

Figure 1.2: Summary of types of peel test configurations (modified) [5].

While there are a variety of different set ups for the peel test, they are all governed by a few key equations. These equations mainly revolve around the concept of energy conservation as well as Griffith's criteria. Considering the basic peel test set up where a flexible adhesive is peeled off a rigid substrate, Kendall formulates Equation 1.1 [6]:

$$\left(\frac{F}{b}\right)^2 \frac{1}{2dE} + \left(\frac{F}{b}\right) (1 - \cos\theta) - R = 0 \quad (1.1)$$

where  $F$  is the force applied to the tape,  $b$  is the width of the tape,  $d$  is the thickness of the tape,  $E$  is Young's Modulus of the tape,  $\theta$  is the angle between the tape and the rigid substrate, and  $R$  is the work of adhesion. Through rearranging this equation and more specifically defining the work of adhesion as the strain energy release rate ( $w$ ), Equation 1.2 is formulated:

$$\frac{F}{b} = -dE(1 - \cos\theta) \pm \sqrt{d^2E^2(1 - \cos\theta)^2 + 2dEw} \quad (1.2)$$

This equation can be used to determine the required peel force ( $F$ ) or peel angle ( $\theta$ ) based on the geometric properties of the adhesives as well as the intrinsic properties of the material itself. Figure 1.3 illustrates the basic geometry of the traditional peel test set up. This graphic includes important physical parameters such as the thickness ( $d$ ) and width ( $b$ ) of the adhesive as well as controllable experimental variables such as the peel force ( $F$ ) and peel angle ( $\theta$ ) that are seen in the governing equations.

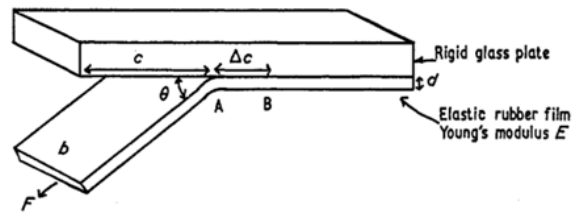


Figure 1.3: Traditional peel test geometry [6].

### 1.3.2 Peel Test Applications

While there are a variety of peel test set ups and applications, each system is governed by the same basic peeling geometry and mechanical equations. This allows for creative applications of the peeling motion while maintaining the simple analysis of such motion through returning to the basic geometry and equations.

One interesting application of these basic peel test set ups is seen in a study by Camara et al., which involves the exploration of the relationship between peeling Scotch tape and the generation of x-rays [7]. In the experimental set up shown in Figure 1.4, there is simultaneous winding and unwinding of a roll of tape. Driven by a motor, a roll of tape is unwound and rewound around another spool a set distance away. This setup allows for a fixed location of the peel front, a constant peel angle, control over the required force and separation speed through motor controls, and simple measurements of the movement of the system through an encoder. This is a less traditional setup for peeling, but it allows for the control of several important variables of the system while maintaining the basic peeling geometry.

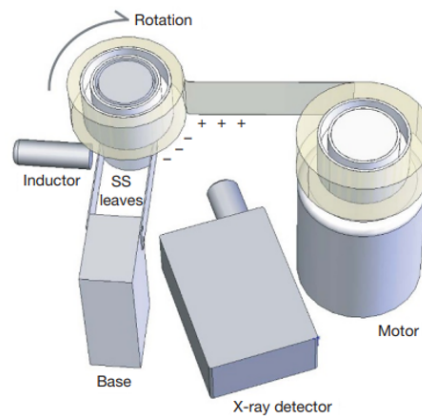


Figure 1.4: X-ray generation set up [7].

The relationship between separation speed and the generation of charge has been previously explored through a study conducted by Zhang et al. [8]. As depicted in Figure 1.5, a peel test is performed with a discontinuous electrode in the place of the continuous rigid substrate the adhesive is traditionally peeled from. The electrode has a grid pattern of alternating regions of material and vacancies. As the peel front propagates, instabilities are created at the transitions between regions

of material and void. The adhesive quickly jumps out of contact with the electrode, resulting in a faster separation speed. The current is measured as the tape is unpeeled, with jumps in current corresponding to these transition point instabilities. This phenomenon is explained through the lens of energy conservation, energy dissipation area, and the peel test. The slower peel speed allows the material to creep, and the mechanical energy from peeling is converted to the internal energy that goes into the deformation of the material. In contrast, when a material is peeled at a faster speed at these transition point instabilities, there is no time for the material to creep. The mechanical energy that goes into peeling is converted into other forms of energy, including electrical energy.

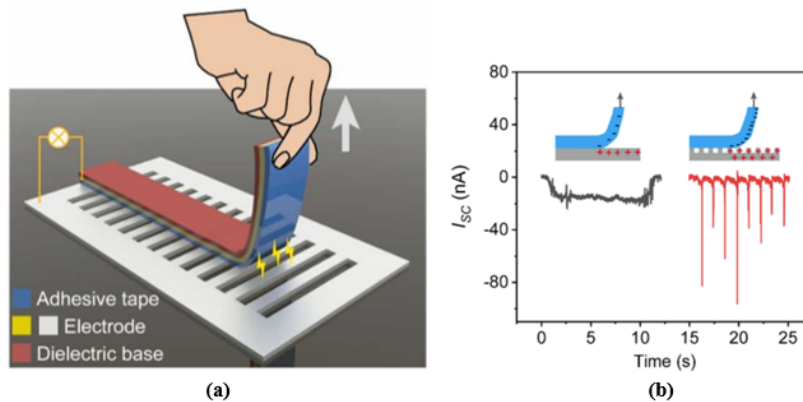


Figure 1.5: (a) Experimental configuration and (b) results from study by Zhang et al. [8].

Traditional peel test geometry and equations serve as the foundation for this thesis research through combining the fundamental mechanical equations generated by Kendall [6] and the experimental set up seen in the study by Camara et al. [7]. Camara et al.'s set up of simultaneous winding and unwinding of an adhesive offers convenient mechanical control over the variables that are integrated into Kendall's equations, allowing for better control and understanding of the interaction of variables within the system. This framework also provides a simple, automated experimental set up which can enhance repeatability in the trials and maximize control over the system.

While this thesis explores similar concepts of separation velocity and charge generation seen in the work by Zhang et al. [8], there will be different assumptions in place as well as experimental constraints. The adhesive material that will be used in this experiment will be assumed to be perfectly elastic. The deformation and creep seen in the experiments conducted by Zhang et al. will not be considered, leading to alternative energy balance equations. Also, this thesis consists of a peel test with a continuous adhesive surface. No changes will be observed at the adhesive interface, and there will be constant contact between the adhesive and the rigid substrate. This constraint eliminates certain external factors related to the adhesive interface since it remains constant. Underlying guiding principles between the two studies are also different. Zhang et al.'s study focuses mostly on balances between the different forms of energy transformed within the system, while this thesis aims to relate the separation speed to the generated charge through pure mechanics.

# Chapter 2

## Methods and Materials

This chapter presents the experimental procedures utilized in this thesis. Details are provided on the execution of experiments, the design of the experimental set ups, and the measurement techniques utilized to collect data for specific parameters. The two parameters measured through experimentation are the adhesive peel angle and the magnitude of charge generated during peeling. Each parameter is measured through both a manual and an automatic process, resulting in the utilization of four distinct experimental procedures: 1) the manual angle measurement procedure 2) the automatic angle measurement procedure 3) the manual charge measurement procedure and 4) the automatic charge measurement procedure. Figure 2.1 provides visualization and summary of the experiments conducted in this thesis. The following sections outline the experimental procedures for measuring the peel angle and the charge magnitude, providing details on both the manual and automatic procedures for the measurement of both parameters. The 3D printed components mentioned throughout this chapter were all initially modeled on SolidWorks, and dimensioned sketches of each component can be found in Appendix A.

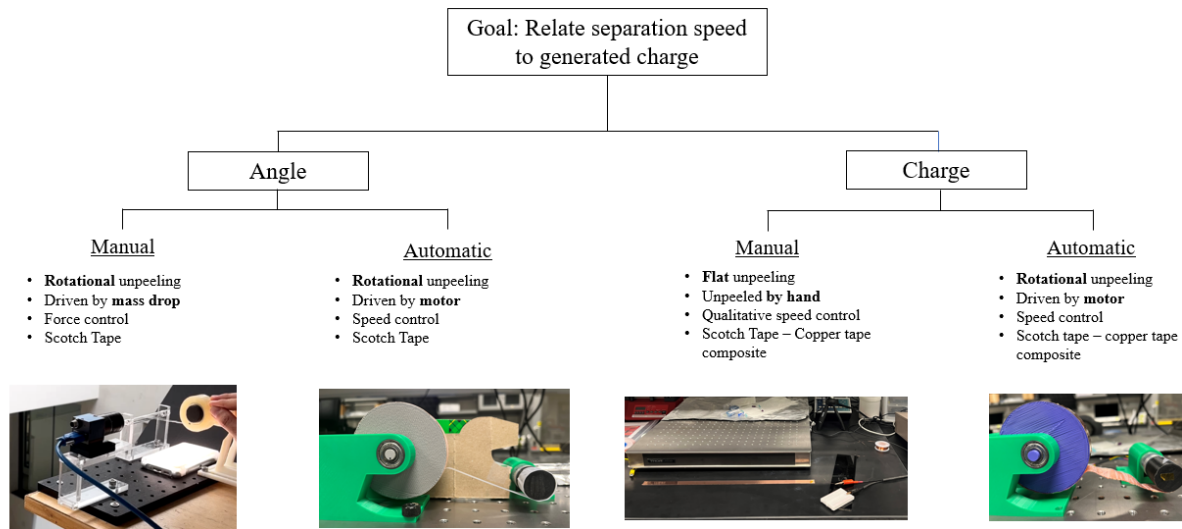


Figure 2.1: Outline of experimental procedures.

## 2.1 Angle Measurement

This section presents the manual and automatic experimental procedures for measuring the adhesive peel angle, which is the angle between the flexible adhesive and the rigid surface from which the adhesive is peeled. This peel angle is a key component in the general peeling equations of motion. Through monitoring the peel angle throughout the peeling process, these general peeling equations of motion can be more easily used to analyze the behavior of the system.

### 2.1.1 Manual Angle Measurement Procedure

The defining characteristic of the manual angle measurement procedure is that peeling is driven by a falling mass. In this experimental set up, a roll of Scotch tape is mounted on a spool. One end of the Scotch tape is secured to a specified mass which is dropped from an elevated surface. As the mass falls, the tape unrolls and unpeels from itself. During unpeeling, a high-speed camera is positioned to capture the side view of the roll of tape. This footage allows for the analysis of the peel angle through post processing, details of which will be provided in a following subsection. The relationship between the peeling force and the resulting peel angle is the focus of this experimental setup.

#### Design of Experimental Set Up

This subsection presents the specifications and materials of the components that comprise the manual angle measurement set up depicted in Figure 2.2. Materials and equipment to fabricate these components are supplied by livMats at the University of Freiburg. The following paragraphs detail each component labeled in Figure 2.2.

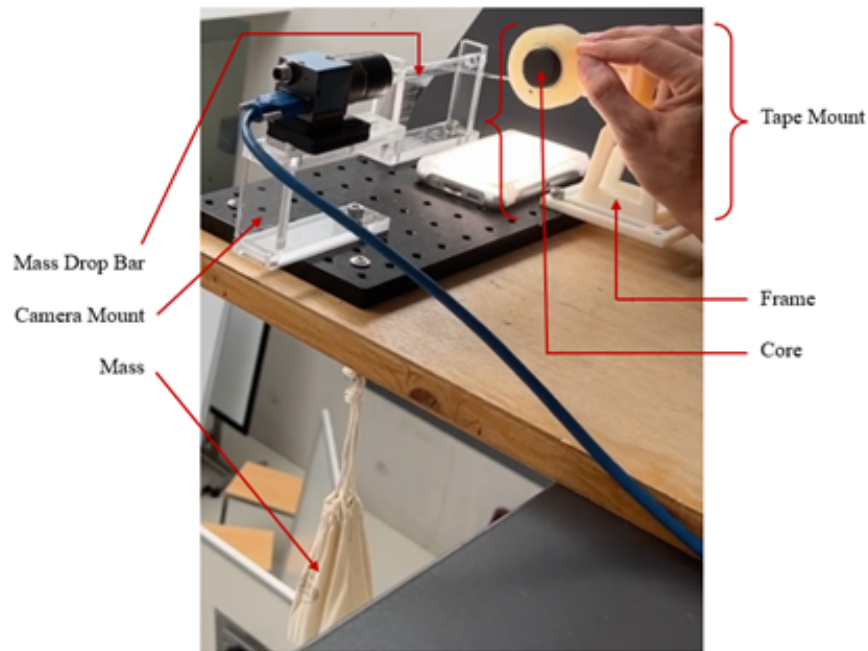


Figure 2.2: Manual angle measurement procedure experimental set up.

The 3D printed tape mount is the component which directly supports the unpeeling process. A premanufactured roll of Scotch tape is mounted on the rotating core which is designed to accommodate the size of the manufactured spool. The rotating core has an outer diameter of 26.5 mm such that a roll of Scotch tape can slide onto the core with a tight fit to avoid slipping during unpeeling. This component was printed using a PLA printer provided by the University of Freiburg. The frame has an overall height of 106 mm, a width of 64 mm, and a length of 126 mm. Many solid bodies and faces of the frame are hollowed to allow for the conservation of material and minimization of 3D print time. The frame was printed on a Stratasys printer. The core interfaces with the frame via two ball bearings embedded in the frame. The core is only supported on one side by the frame, with a central rotational axis extruding from one face of the core to interface with the ball bearings in the frame.

Once the roll of Scotch tape is secured on the tape mount, the Scotch tape is partially unrolled and fed around the top of the mass drop bar. The roll of Scotch tape is positioned on the tape mount such that the non-adhesive side of the tape comes in contact with the mass drop bar. The mass drop bar is fabricated using laser cut acrylic.

The mass used to perform these trials consists of 1 kg metal cubes placed in a cloth drawstring bag. The mass and consequent peel force can be variable depending on how many cubes are placed in the drawstring bag. The strings of the drawstring bag are tied to a plastic component to which the tape is wrapped around and secured. This plastic component is a cylindrical piece of acrylic that was laser cut to size. The mass is dropped from a second story window onto a pile of scrap Styrofoam, which aims to minimize damage on impact.

The camera mount consists of acrylic components that were laser cut to accommodate a high-speed camera. The high-speed camera is directly screwed to this acrylic mount, mounted in such a

way to obtain a side view of the tape unpeeling.

### Angle Measurement

The peel angle in the manual angle measurement procedure is dependent on the overall physical geometry of the experimental set up, such as the placement of the mount in relation to the mass drop bar as well as the radius of the core. Figure 2.3 illustrates these geometric relationships, with  $\theta$  representing the peel angle present in the traditional peel test and the Kendall peeling equations [6]. Through analyzing the videos captured by the high-speed camera during the unpeeling process using the Kinovea video processing software, the angle ( $\alpha$ ) is measured for each frame of the video. This measured angle ( $\alpha$ ) along with the spatial geometric relations of the experimental set up are utilized to calculate the peel angle ( $\theta$ ) through Equations 2.1-3.

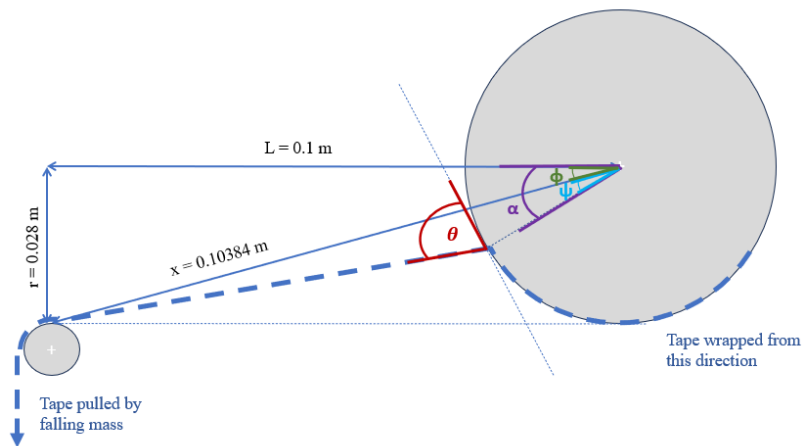


Figure 2.3: Geometry relating measured experimental angle ( $\alpha$ ), traditional peel angle ( $\theta$ ), and physical set up geometry of manual angle measurement procedure.

$$\phi = \tan^{-1} \left( \frac{r}{L} \right) \quad (2.1)$$

$$\psi = \alpha - \phi \quad (2.2)$$

$$\theta = \text{acot} \left( \frac{\frac{r}{L} - \cos\psi}{\sin\psi} \right) - 180^\circ \quad (2.3)$$

### 2.1.2 Automatic Angle Measurement Procedure

The use of a rotational motor is the defining characteristic of the automatic peeling experimental setup. Figure 2.4 depicts this automatic peeling setup and labels its main components. In this setup, Scotch tape is wound around two spools, one of which rotates freely (the tape spool) and the other of which is driven by a rotational motor (the motor spool). As the motor rotates, the Scotch tape is unwound from the tape spool and rewound the motor spool. The unwinding of the

Scotch tape from the tape spool is the peeling process analyzed and equated to traditional peeling methods. Utilizing Arduino, the rotational speed of the motor can be controlled, resulting in the ability to unpeel the tape at different speeds.

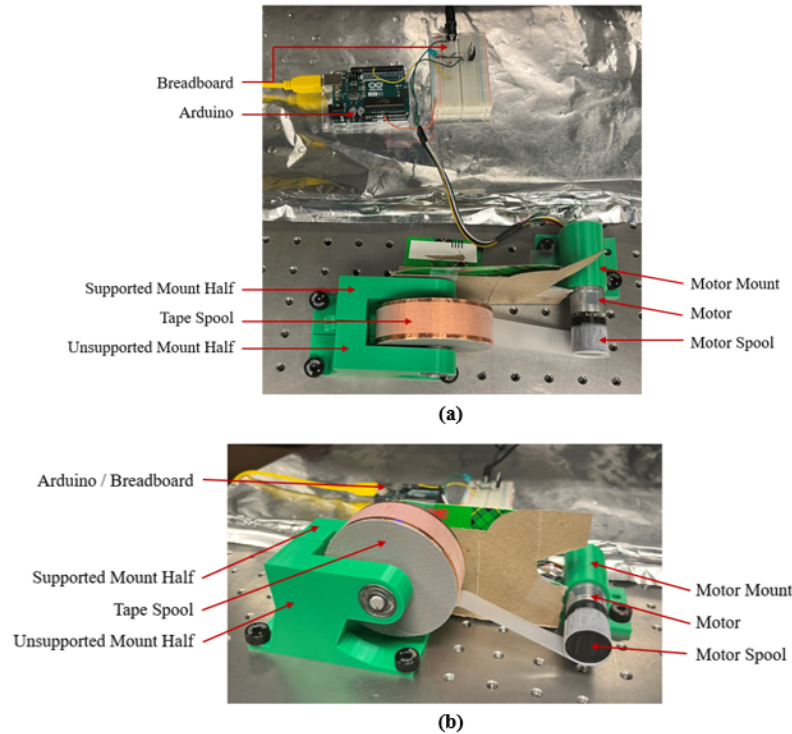


Figure 2.4: The (a) top view and (b) front view of the automatic angle measurement procedure experimental set up.

### Design of Experimental Set Up

This subsection presents the materials and specifications of the different components from which the automatic peeling experimental setup is comprised. A combination of 3D printed components, purchased hardware, circuit elements, and software are included in this automatic experimental setup. All 3D printed components described in this section are printed on an Original PRUSA MK4 PLA printer with a 15% infill. These resources are accessible at the Penn State Learning Factory. All components for this experimental setup are mounted on a Thorlabs metal mounting surface with the compatible thumb screws.

The tape spool is the 3D printed component which the Scotch tape is initially wound around. The larger, cylindrical portion of the spool which the tape is wound around has a diameter of 80 mm and a thickness of 25 mm. The smaller cylindrical axis of the spool rotates within the supported and unsupported mount halves. This component has a diameter of 7.95 mm and extrudes from either face of the larger cylinder by 20 mm.

The supported and unsupported mount halves are the stationary components within which the tape spool rotates. These components have an overall height of 67.5 mm, width of 30 mm, and length of 110 mm. This results in the bottom edge of the tape spool being held 12.5 mm above



the surface when it is properly set in the mount halves. Rather than having one continuous spool mount, there are instead the supported and unsupported mount halves to allow for easy removal and replacement of the tape spool. These halves are not mirror images of each other. The supported half has an additional vertical component under the overhang to minimize any potential vibrations that may arise due to the rotation of the spool and unpeeling of the tape. The unsupported mount half does not have this additional vertical support. This allows for the unobstructed view of the spool while unpeeling as the additional vertical support would cover key portions of the spool, obstructing the video needed for imaging and quantifying. The supported mount half is farthest from the camera and the unsupported mount half is closest to the camera. This allows for the minimization of vibrational instabilities while peeling owing to the supported mount half while simultaneously having an unobstructed view of unpeeling due to the presence of the unsupported mount half.

The tape spool interfaces with the mount halves via four 608 2RS B deep groove ball bearings, with two ball bearings secured in each mount half. On the tape spool axis, there are four washers, two on either side of the larger cylinder, to minimize the lateral movement of the tape spool within the bearings of the mount halves. The tape spool is covered with a single layer of copper tape.

The unpeeling process is driven by a Bemonoc 12 V high speed DC gear motor with integrated hall encoder. This motor has a maximum no load speed of 600 rpm and a rated torque of 0.25 kg-cm. Throughout this thesis, motor speeds of 150 rpm and 250 rpm are utilized. The rotational motor is mounted in a 3D printed motor mount. The motor mount has an inner diameter of 24.70 mm to allow for a snug fit of the motor inside to minimize disturbances but allow for the easy removal of the motor if needed. The mount has an overall length of 50 mm and height of 40 mm, resulting in the rotational axis of the motor being held 25 mm off the surface.

The 3D printed motor spool is mounted on the rotational end of the motor. This spool rotates at the input motor rpm and is the component which the Scotch tape is rewound upon once it is unpeeled from the tape spool. This motor spool has a diameter of 25 mm and a width of 25 mm. The inner geometry of the spool matches the geometry of the rotational component of the motor, having a tight fit to minimize discrepancies between motor rotation and spool rotation.

The rotational motor and Arduino interface through a breadboard circuit, the configuration of which is detailed in Appendix B. This set up consists of two power supplies. A laptop computer drives the Arduino functionality while a 100-240V 1A DC power supply adapter provides 12V to the rotational motor. The speed of the rotational motor is determined by an Arduino code, which is provided in Appendix C.

## Angle Measurement

The rotational peeling geometry is related to the traditional peel test geometry through the measurement of certain angles present in the automatic peeling setup. These angles are measured through analyzing videos which capture the front view of the tape spool as the tape is unpeeling. Using Kinovea video processing software, specific angles throughout each trial are measured frame by frame for the duration of the trial. This raw data is then uploaded to MATLAB for further analysis.

Figure 2.5 illustrates the key angles utilized in the geometric conversion from rotational peeling to the traditional flat surface peeling. The angle of the unpeeled tape with respect to the tangent of the spool at the point from which the tape releases from the spool, labeled in Figure 3 as  $\theta$ , is equal

to the peel angle measured in traditional peel tests. To obtain a value for  $\theta$  as the tape unpeels,  $\alpha$  and  $\psi$  are measured in each frame of the video during post processing. These angles are then used in Equations 2.4 and Equation 2.5 to obtain a value for  $\theta$  for each frame of the video. The bridge between rotational unpeeling and traditional peel tests is the value of  $\theta$ .

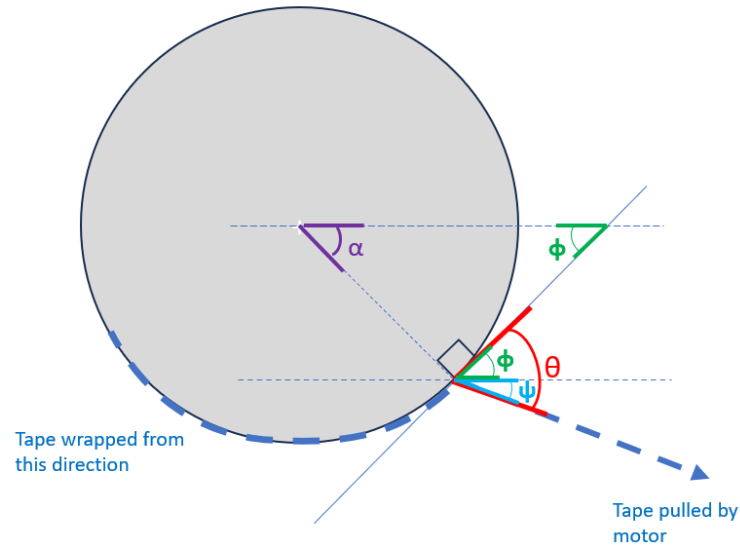


Figure 2.5: Geometry relating measured experimental angles ( $\alpha$ ,  $\psi$ ) to traditional peel angle ( $\theta$ ) for automatic angle measurement procedure.

$$\phi = 90^\circ - \alpha \quad (2.4)$$

$$\theta = \psi + \phi \quad (2.5)$$

## 2.2 Charge Measurement

This section presents the experimental procedures utilized to measure the charge generated during the peeling process. Similar to the measurement of the peel angle, the charge is measured using both a manual and automatic peeling. In both the manual and automatic peeling processes, the adhesive being peeled is a Scotch tape-copper tape composite consisting of copper tape being layered on top of Scotch tape. The manual and automatic peeling processes are also similar in that a Keithley electrometer is used to measure generated charge. The positive lead of the electrometer is connected to one end of the Scotch tape-copper tape composite and the negative lead is connected to ground.

### 2.2.1 Manual Charge Measurement Procedure

The defining characteristics of the manual peeling process is that the adhesive is peeled by hand from a flat surface. The Scotch tape-copper tape composite of length 55 cm is mounted to a

flat acrylic surface. This set up is seen in Figure 2.6. The adhesive is then peeled by hand at both “slow” and “fast” rates. While this is done by hand, steps are taken to ensure as much consistency as possible. “Slow” trials aim to peel the length of the adhesive over the course of 8 s while “fast” trials consist of peeling over the course of 1 s. The end of the adhesive does not come out of contact with the acrylic surface; the peeling stops before the end of the adhesive to ensure that it remains stuck to the acrylic surface. Five trials for “slow” peels and six trials for “fast” peels are performed. A copper wire is connected to the positive lead of the electrometer and the stationary end of the tape composite that does not come out of the acrylic surface.

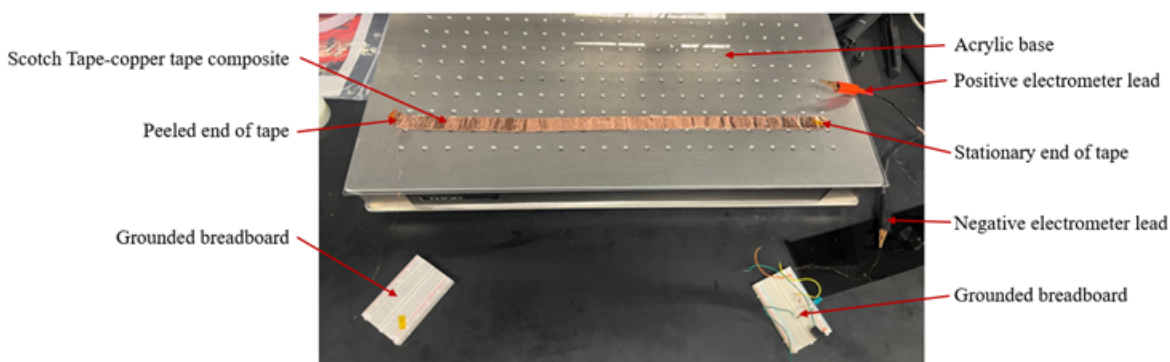


Figure 2.6: Manual charge measurement procedure experimental set up.

### 2.2.2 Automatic Charge Measurement Procedure

The automatic charge measurement procedure uses the same experimental set up as the automatic angle measurement procedure described in the previous section and seen in Figure 2.4. The Scotch tape-copper tape composite is mounted on the tape spool and unwound by the Bemonoc 12V high speed DC gear motor. Motor speeds of 150 rpm and 250 rpm are utilized, with five trials for each speed conducted. A copper wire is connected to the end of the Scotch tape-copper tape composite that is initially stuck to the motor spool. The copper wire is fed from the end of the tape composite to the center of the circular face of the motor spool where it is then secured and connected to the positive lead of the electrometer. It is secured in this location to minimize movement of the wire as much as possible during unpeeling.

# Chapter 3

## Results and Discussion

### 3.1 Angle Measurements

This section presents the data collected for the peel angle for both the manual and automatic peeling process. The angle measured in both procedures is related to the peel angle ( $\theta$ ) analyzed in traditional peel test procedures depicted in Figure 1.3.

#### 3.1.1 Manual Angle Measurements

As described in Chapter 2 Section 2.1.1, the manual angle measurement procedure consists of unwinding a roll of Scotch tape via a falling mass attached to one end. The angle from which the tape detaches from the roll as it unpeels is measured in video post processing. Masses of 0.555 kg and 1.500 kg are utilized in this thesis for unpeeling, and the respective peel angles are measured. Figure 3.1 depicts the measured peel angle for four trials utilizing a drop mass of 0.555 kg. This figure illustrates a downward trend for the peel angle as the tape is unpeeled over the course of about one second, with an initial angle of about  $90^\circ$  and a final angle of about  $40^\circ$ . Slight oscillations over the course of each trial are also seen. This trend remains consistent over all four trials utilizing the 0.555 kg drop mass. The peel angle resulting from utilizing a 1.500 kg drop mass is depicted in Figure 3.2. Over the course of the one second unpeeling, downward sloping oscillations are visible within the peel angle measurements, with initial values of around  $90^\circ$  and final values of around  $40^\circ$ . The two different drop masses yield relatively similar results for peel angle, seen in Figure 3.3. There is a consistent downward, oscillating trend for the peel angle which stays within the range of  $90^\circ$  to  $40^\circ$ . However, the peel angle for the 1.500 kg mass drop experiences larger, clearer oscillations as it unpeels compared to the 0.555 kg mass drop.

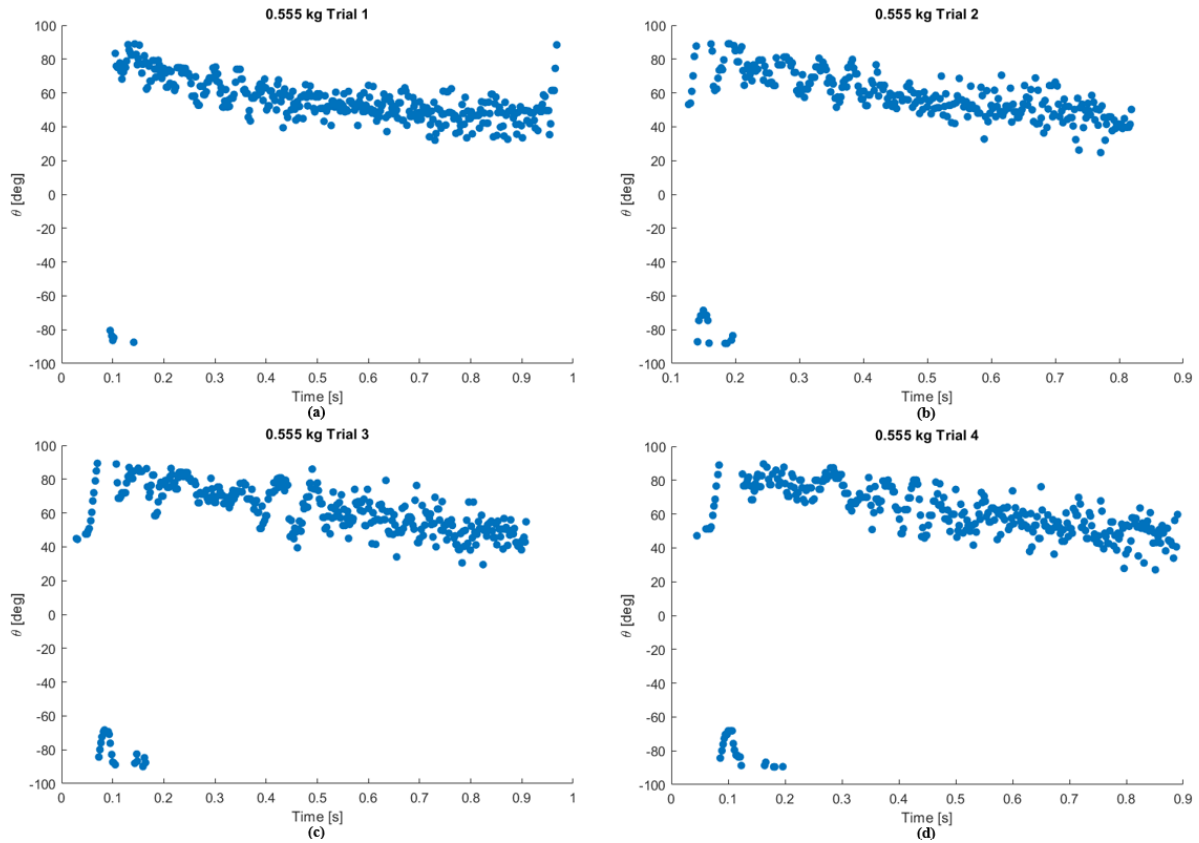


Figure 3.1: Peel angle ( $\theta$ ) measurements for (a-d) four trials for manual angle measurement procedure with a 0.555 kg drop mass.

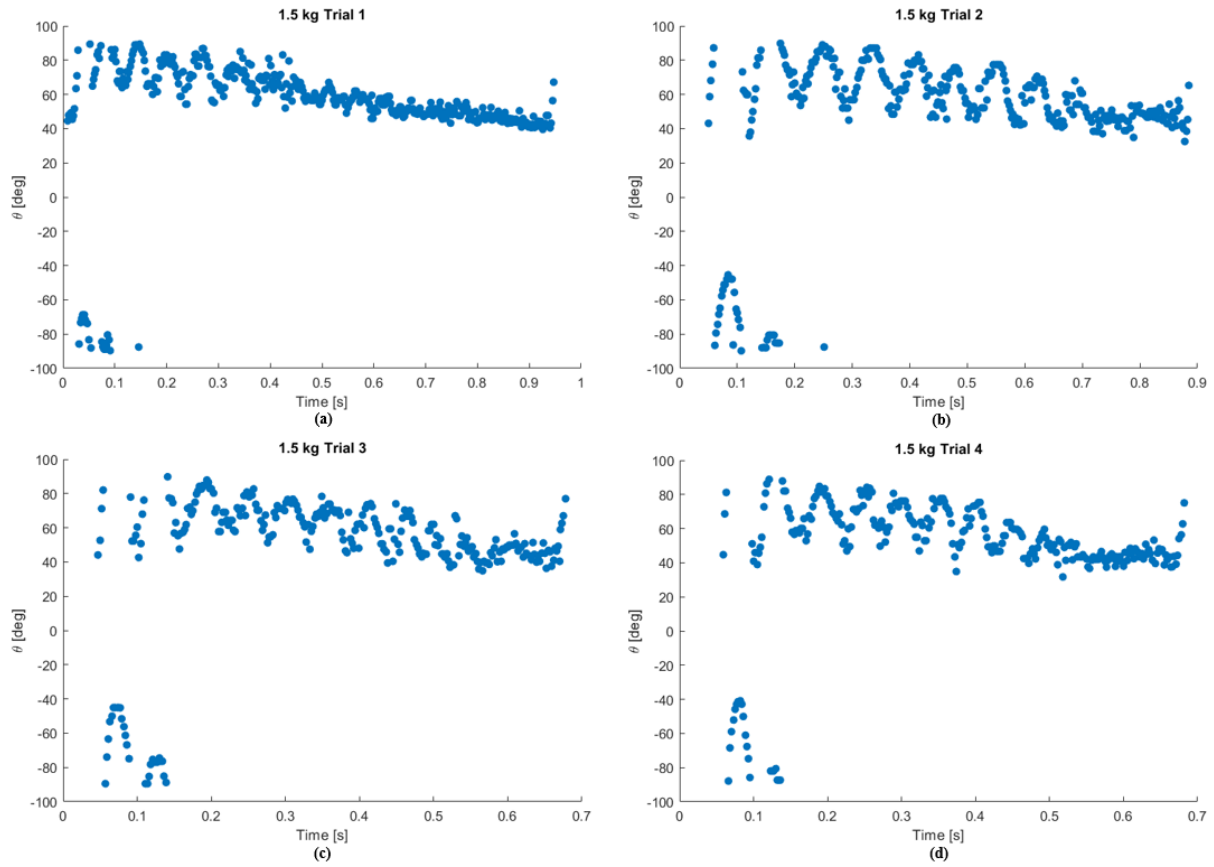


Figure 3.2: Peel angle ( $\theta$ ) measurements for (a-d) four trials for manual angle measurement procedure with a 1.500 kg drop mass.

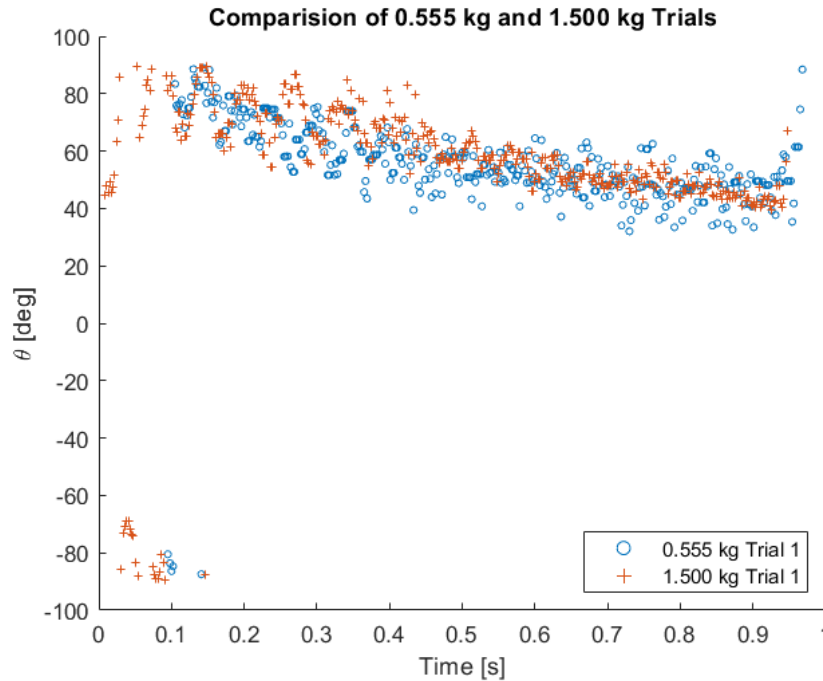


Figure 3.3: Comparison of peel angle ( $\theta$ ) for 0.555 kg and 1.500 kg trials.

There are several explanations for the occurrence of the oscillating peel angle. Vibration and instability inherent with the physical set up could be one cause for the appearance of the oscillations. If the tape mount vibrates as the Scotch tape unpeels, this vibration may materialize as an oscillating peel angle. The stick-slip regime associated with adhesive peeling offers an additional explanation for the presence of oscillations in the peel angle. As an adhesive is unpeeled, the peel front transitions from periods of extended sticking followed by periods of brief unpeeling, or “slipping” [9]. This non-uniform peeling could result in an unsteady oscillating peel angle. In addition to causing non-uniform peeling, the adhesive stick-slip regime can potentially explain the larger oscillations seen in the trials with a 1.500 kg drop mass. As the peel velocity increases, the amplitude of the “stick” and “slip” periods increases [9]. Since the tape attached to the 1.500 kg mass is unpeeling with a faster velocity, the larger oscillations compared to the 0.555 kg trials could be due to the characteristics of the adhesive stick slip regime.

### 3.1.2 Automatic Angle Measurements

The data for the automatic angle measurements is seen in Figure 3.4. Two motor speeds, 150 rpm and 250 rpm, are utilized in this procedure with three trials performed at each motor speed, as discussed in Chapter 2. Figure 3.4a depicts peel angle data collected from three trials utilizing a motor speed of 150 rpm. The peel angle remains consistently between 85-90° from the beginning to the end of the trial, without much variation between trials. Peel angle measurements for three trials utilizing a motor speed of 250 rpm are seen in Figure 3.4b. Data trends between trials of the same motor speed are relatively consistent, with each trial beginning with a very unpredictable and chaotic peel angle but eventually converging after about 2.5 s within the range of 85-90°. Figure 3.4c shows that both speeds result in the peel angle converging to the range of  $90 \pm 5^\circ$ .

However, trials performed at higher speeds take longer for the peel angle to converge into this range. The adhesive stick-slip regime may explain the initial chaos at the beginning of the 250 rpm trials. Rapid and sudden acceleration at the beginning of the trial may materialize in the form of an unsteady peel front and consequent chaotic peel angle.

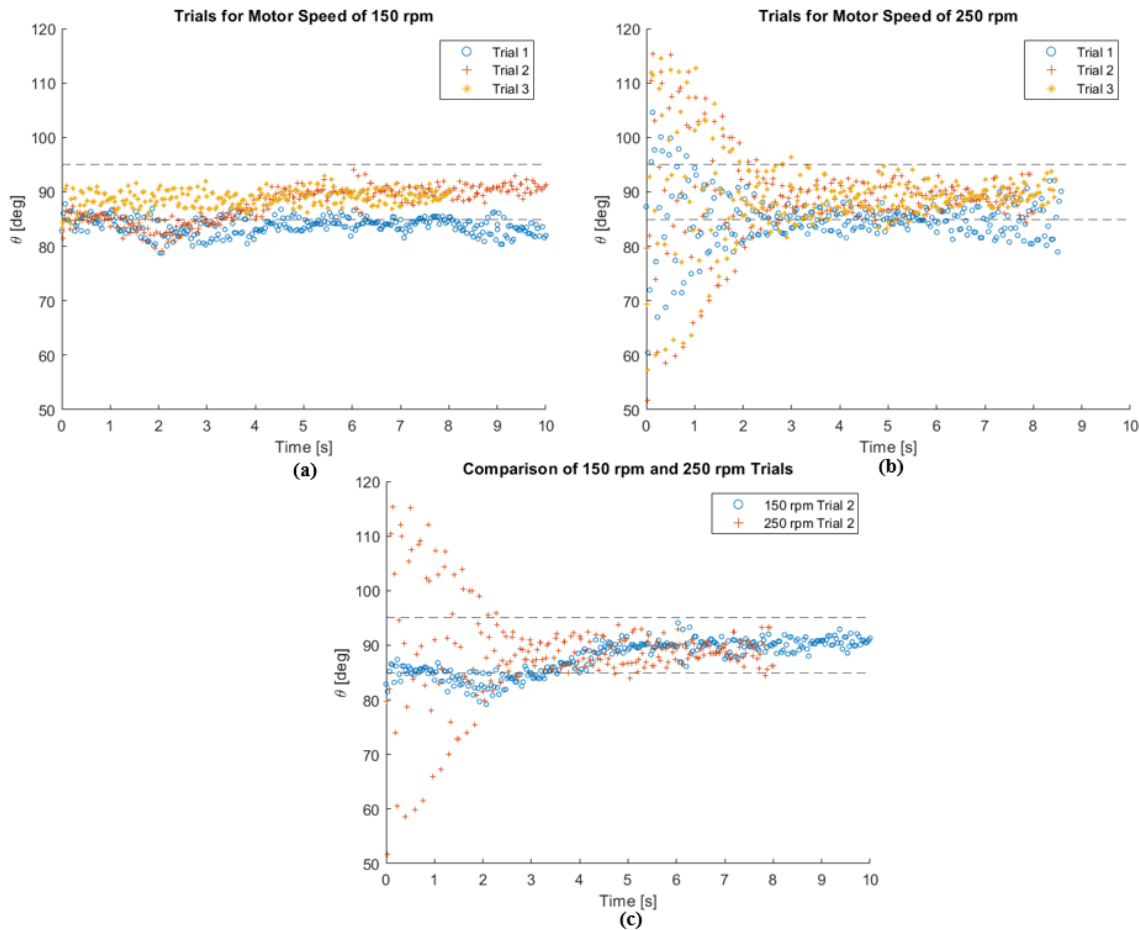


Figure 3.4: Peel angle measurements from automatic angle measurement procedure with a motor speed of (a) 150 rpm and (b) 250 rpm as well as (c) a comparison between the two speeds.

## 3.2 Charge Measurements

This section presents the data collected for the charge, utilizing both the manual and automatic charge measurement procedures as described in Chapter 2 Section 2.2.

### 3.2.1 Manual Charge Measurements

The manual charge measurement procedure was utilized to collect the data seen in Figure 3.5. Trials were conducted at both the “slow” and “fast” speeds, both yielding relatively consistent results on the scale of  $0.1 \mu\text{C}$ . Figure 3.5a shows the results for the “slow” trials. As can be seen, the “slow” trial yields charge measurements that consistently level off at around the  $-0.25$



$\mu\text{C}$  mark after the approximately 8 s peel. Figure 3.5b shows that the “fast” trials also yield relatively consistent results in that each trial levels off below the  $-0.25 \mu\text{C}$  mark. Figure 3.5c offers a comparison between the “slow” and “fast” trials, suggesting that the faster separation speed yields a larger magnitude of charge generated.

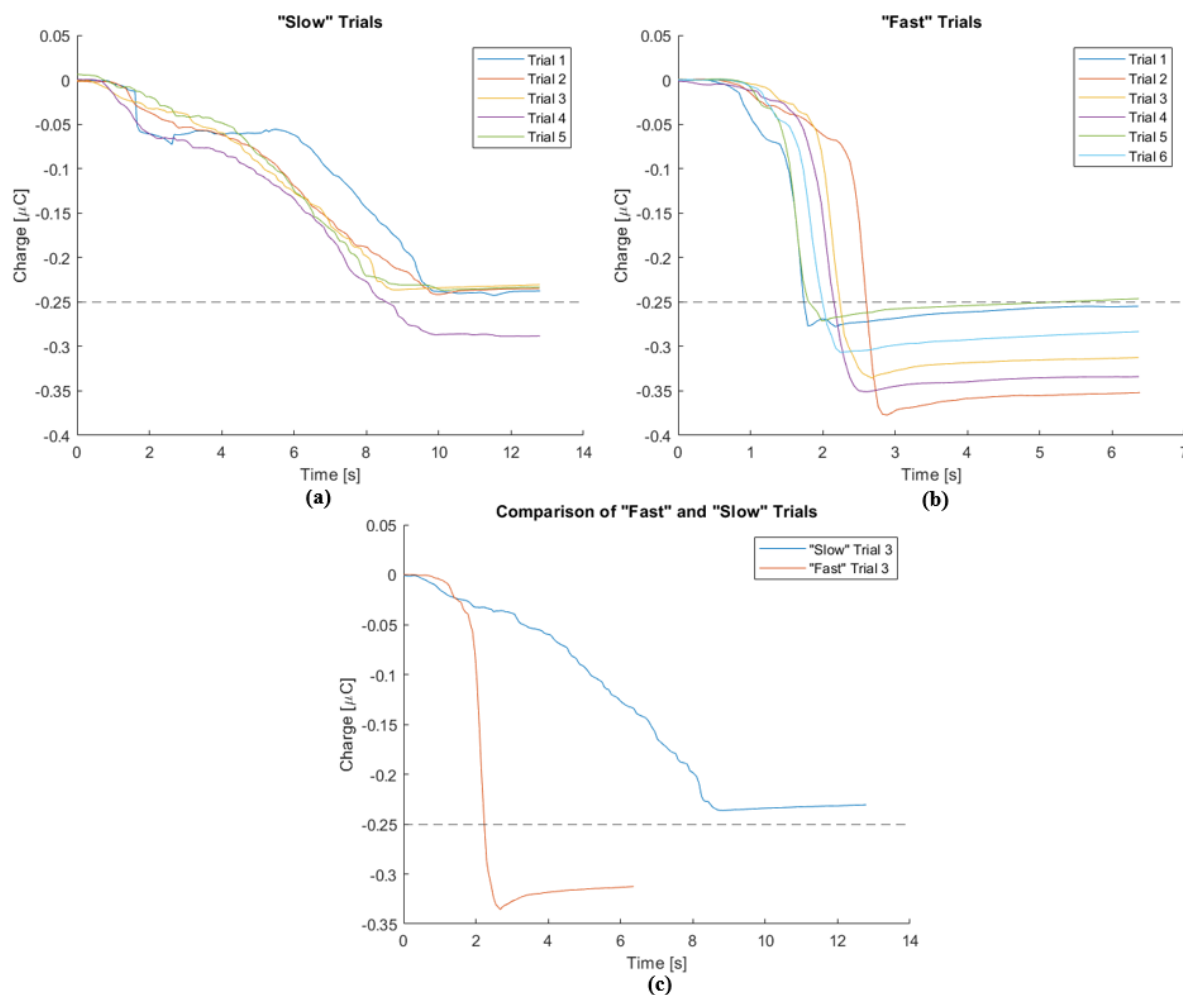


Figure 3.5: Charge measurements from manual charge measurement procedure for (a) “slow” trials and (b) “fast” trials as well as (c) a comparison between speeds.

### 3.2.2 Automatic Charge Measurements

The automatic charge measurement procedure yielded five trials for motor speeds of both 150 rpm and 250 rpm, with the charge data presented in Figure 3.6. The charge measurements collected for the trials conducted with a motor speed of 150 rpm are seen in Figure 3.6a. As seen in this figure, charge values on the scale of  $0.001 \mu\text{C}$  are generated. A loosely consistent trend is seen between three of the five trials graphed in this figure, but overall, there is a lack of consistency. There is even less consistency between trials conducted at the 250 rpm motor speed, as seen in Figure 3.6b. These trials also yielded charge measurements on the scale of  $0.001 \mu\text{C}$ , but there is no general trend seen between trials. Figure 3.6c presents a comparison between the 150 rpm

and 250 rpm trials, showing that the 250 rpm trials yielded smaller charge values than the 150 rpm trials. This could be due to the fact that there is less external motion in the physical set up in the slower 150 rpm trials. The wire that connects the Scotch tape-copper tape composite to the electrometer lead experiences the rotations of the motor, potentially influencing the charge readings gathered by the electrometer. This extra motion could cause the charge measurements to be lower than the actual magnitudes of charge present during the trials. During the slower 150 rpm trials, the wire experiences less motion compared to the 250 rpm trials, yielding slightly more consistent and potentially more accurate results.

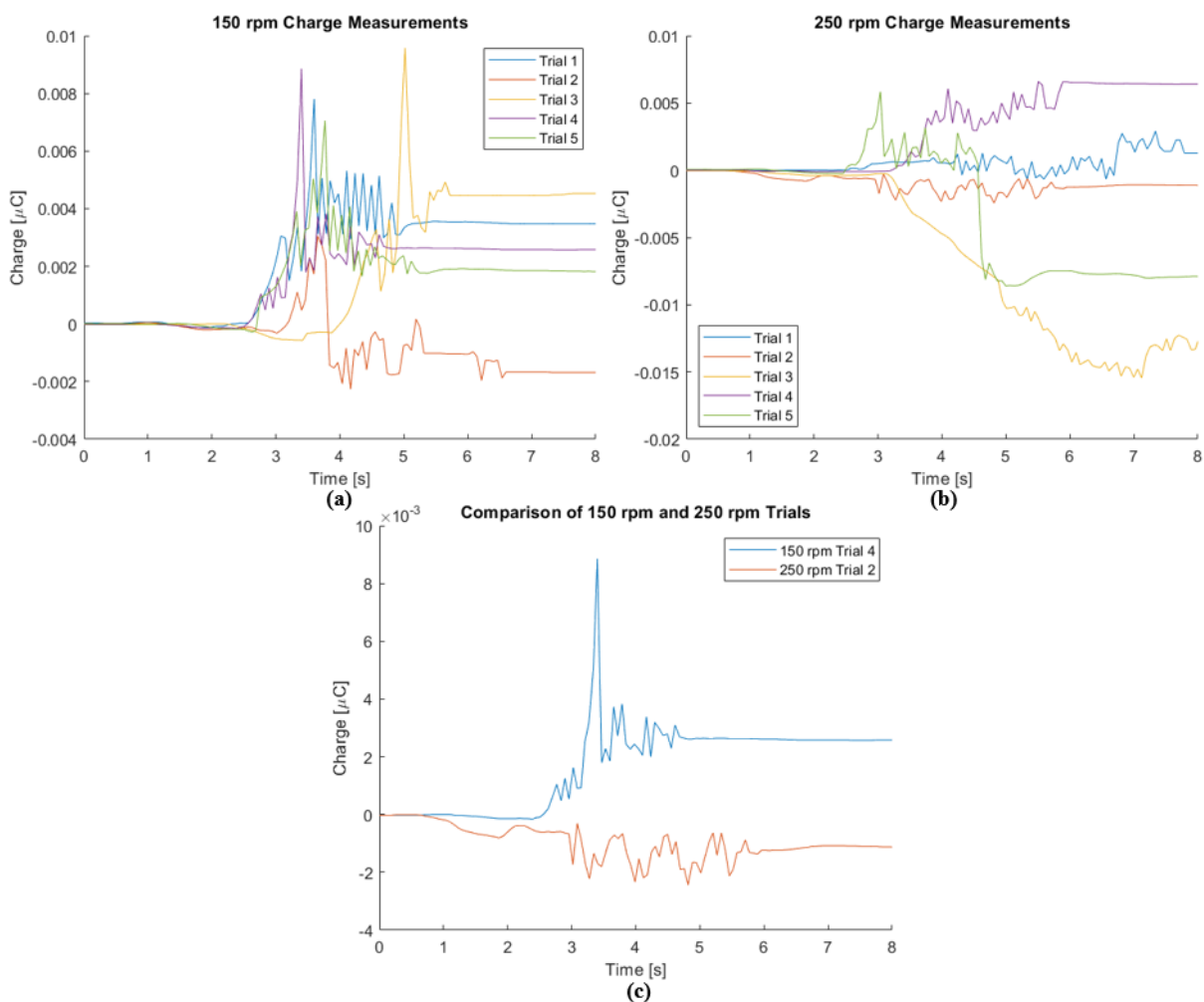


Figure 3.6: Charge measurements from automatic charge measurement procedure for (a) motor speeds of 150 rpm, (b) motor speeds of 250 rpm, and (c) a comparison of 150 rpm and 250 trials.

# Chapter 4

## Conclusions and Future Work

### 4.1 Conclusions

The broad goal of this thesis research is to use the mechanics of peeling to relate the generation of triboelectric charge to the separation speed of two surfaces. Four experimental procedures are developed to measure peel angle and charge generated, with their geometries analyzed to parallel that of traditional peel tests. The data gathered by each procedure evaluated the correlation between both peel angle and generated charge to an enacted peel speed, which provided insights on the overall investigation of separation speed and triboelectric charge generation as well as the most effective methods to investigate this relationship.

By developing the experimental set ups based on traditional peeling geometry, the first objective of imposing simple mechanics on a triboelectric system is achieved. While traditional peel tests consist of peeling a flexible adhesive from a flat rigid substrate, this thesis successfully employed rotational peeling. Through recording each trial and measuring key angles, post-processing proved to be a reliable way of measuring the peel angle ( $\theta$ )—a foundational variable in all fundamental peeling equations. While peeling mechanics proved to be transferable and applicable in this context, complex properties of adhesion were inherently introduced. The stick-slip regime present in adhesive peeling materializes in the experimental data. This stick-slip regime is particularly influential in the angle measurements, presenting itself in the form of oscillations and convergence time. Adhesive properties may also influence the charge measurements given the ambiguities surrounding the charge transferring mechanism as discussed in Chapter 1. In general, imposing peeling mechanics successfully allowed for the control of the physical experimental parameters such surface separation angle ( $\theta$ ), force of separation ( $F$ ), and separation speed. However, this comes at the cost of introducing the complex behavior inherent to adhesives.

Experimental procedures utilizing slower peel speeds and uniform test specimen enabled the second objective of maximizing consistency and repeatability. Initially, development of automatic

experimental procedures was the aim of this objective. The manual and automatic angle measurement procedures yielded equally consistent results while the manual charge measurement procedure yielded more consistent results than the automatic charge measurement procedure. Rather than the automation of experimental procedures, the speed at which a trial is conducted proved to be the most influential factor in maximizing repeatability. For both the automatic and manual procedures for both angle and charge measurements, the trials conducted at slower speeds yielded more consistent results. An additional factor that influenced consistency and repeatability is the fabrication and mounting of the material specimens. Any inconsistencies in the tape, such as a wrinkle or air bubble, heavily affected both the angle and charge measurements. Consistency between specimen and properly mounting them on the unpeeling apparatus is very important in achieving this objective. Overall, slower trial speeds and uniform specimen fabrication and mounting were found to be important components of procedures that yielded the most consistent and repeatable results.

In conclusion, this thesis first developed a procedure for a rotational peel test which related peel angle, peel speed, and generated charge through equating rotational peeling geometry to traditional flat peeling geometry. This is significant because well-established traditional peeling equations typically only applied to flat peeling can be applied to rotational peeling, which is a process that is easier to control and automate. Second, procedures to measure charge during peeling were moderately successful. Through the experimental procedures utilized in this thesis, charge measurements were gathered at different peel speeds. While these results are not as consistent and repeatable as desired, it marks an important step in relating separation speed to the magnitude of generated charge. To achieve the broad goal of this thesis, namely relating the speed of separation of two surfaces to the magnitude of charge generated, additional experiments are needed, as discussed in the next section.

## 4.2 Future Work

The development of a method to fabricate consistent and uniform Scotch tape-copper tape composite samples could allow for the reduction of instabilities in the peeling process and yield more consistent results. The current fabrication methods of layering Scotch tape and copper tape by hand is very time consuming and fails to significantly eliminate inconsistencies in the adhesive surface; air bubbles are often seen between the tape and the peeling surface as well as between the Scotch tape and copper tape layers. These air bubbles are due to wrinkles and creases in the copper tape. These wrinkles appear when the composite is initially fabricated and also materialize throughout the peeling process. Given the time-consuming nature of attempting to fabricate the composite without air bubbles or wrinkles, one sample is often used for multiple peeling trials. If a more efficient and more consistent method for fabricating this composite was developed, instabilities during peeling due to air bubbles and wrinkles can be reduced, time can be saved in the fabrication process, and new samples can be used for each trial if desired.

The introduction of a higher torque motor as well as a motor controller into the system will allow for a wider range of trial speeds, more consistency of trial speeds, and the ability to directly explore the relationship between torque and generated charge. Currently, the DC motor employed to unpeel the tape in the automatic peeling processes struggles to overcome the adhesive force of the tape and occasionally stalls rather than unpeels the tape. The output speed is somewhat inconsistent from the input speed given the need for the motor to overcome these adhesive forces, leading

to ambiguities surrounding the true separation speed that prompts the resulting angle and charge outputs. Integrating a motor controller into the system grants more control over the torque and consequent motor speed, which is critical in the exploration of the relationship between separation speed and generated charge.

The exploration of general adhesive properties of the materials used in the described procedures is not directly explored in this thesis yet could have a substantial impact on the relationship between separation speed and generated charge. Adhesion plays a crucial role in every experimental set up throughout this thesis, with adhesion seen between Scotch tape and itself, Scotch tape and copper tape, and Scotch tape and acrylic. The strain energy release rate is a parameter that is present in Kendall's fundamental peeling equations [6], and this parameter would change based on the materials at the interface. Furthermore, triboelectricity is highly dependent on the interaction of the participating surfaces, and the presence of adhesive forces may play a significant role in the behavior of triboelectricity. There are several different surface interfaces throughout these experimental set up, each of which could be further explored.

Purposefully introducing controlled instabilities is another method of exploring the relationship between separation speed and triboelectric charge generation. Instabilities may be introduced into a system through the fabrication of heterogeneous adhesives, which may materialize in the form of variable thickness or stiffness, or the fabrication of a patterned peel surface. Both methods would result in unstable peeling. As the peel front of an adhesive propagates through one of these transition points, either from a stiff to flexible region of a heterogeneous adhesive or over an imperfection in a peeling surface, the separation speed changes. Exploring potential changes in the generation of charge as the peel front navigates these inconsistencies is an additional way to investigate the relationship between separation speed and generation of charge.

## Bibliography

- [1] Wang, Z., Lin, L., Chen, J., Niu, S., Zi, Y., 2016, *Triboelectric Nanogenerators*, Springer International Publishing, Cham, pp. 1-19.
- [2] Lacks, D., Shinbrot, T., 2019, “Long-Standing and Unresolved Issues in Triboelectric Charging,” *Nature Reviews Chemistry*, 3, pp. 465-476.
- [3] Kim, W., Kim, D., Tcho, I., Kim, J., Kim, M., Choi, Y., 2021, “Triboelectric Nanogenerator: Structure, Mechanism, and Applications,” *ACS Nano*, 15(1), pp. 258-287.
- [4] Nazar, A., Egbe, K., Abdollahi, A., Hariri-Ardebili, M., 2021, “Triboelectric Nanogenerators for Energy Harvesting in Ocean: A Review on Application and Hybridization,” *Energies*, 14.
- [5] Bartlett, M., Case, S., Kinloch, A., Dillard, D., 2023, “Peel Tests for Quantifying Adhesion and Toughness: A Review,” *Progress in Materials Science*, 137.
- [6] Kendall, K., 1975, “Thin-Film Peeling—The Elastic Term,” ICI Corporate Laboratory, Cheshire.
- [7] Camara, C., Escobar, J., Hird, J., Putterman, S., 2008, “Correlation Between Nanosecond X-Ray Flashes and Stick-Slip Friction in Peeling Tape,” *Nature*, 455, pp. 1089-1092.
- [8] Zhang, L., Zhang, Y., Li, X., Feng, Y., Yu, B., Zhou, F., 2022, “Mechanism and Regulation of Peeling-Electrification in Adhesive Interface,” *Nano Energy*, 95.
- [9] Dalbe, M., Villey, R., Ciccotti, M., Santucci, S., Cortet, P., Vanel, L., 2016, “Inertial and Stick-Slip Regimes of Unstable Adhesive Tape Peeling,” *Royal Society of Chemistry*, 12, pp. 4537-4548.

# Appendix A SolidWorks Sketches

This appendix presents the dimensioned SolidWorks sketches of 3D printed parts mentioned in Chapter 2. Each component was initially modeled on SolidWorks. The components that comprise the manual experimental set up were printed utilizing resources provided by the University of Freiburg, including a PLA and Stratasys printer. The components that comprise the automatic experimental set up were printed on a PRUSA MK4 PLA printer accessible at the Penn State Learning Factory.

## Manual Experimental Set Up

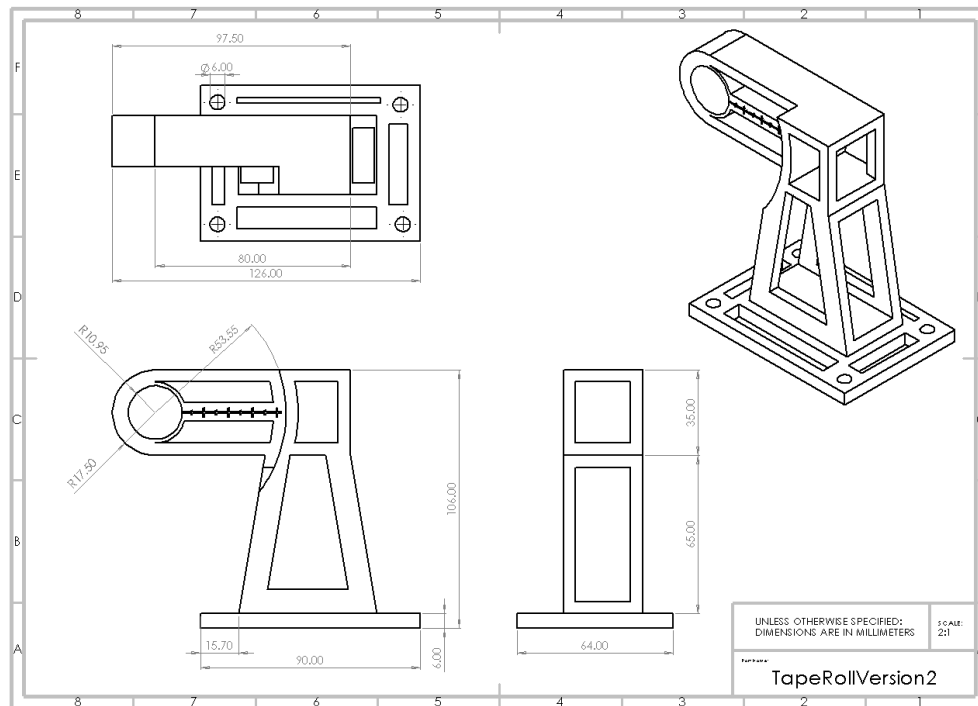


Figure 1: Tape Mount Dimensions.

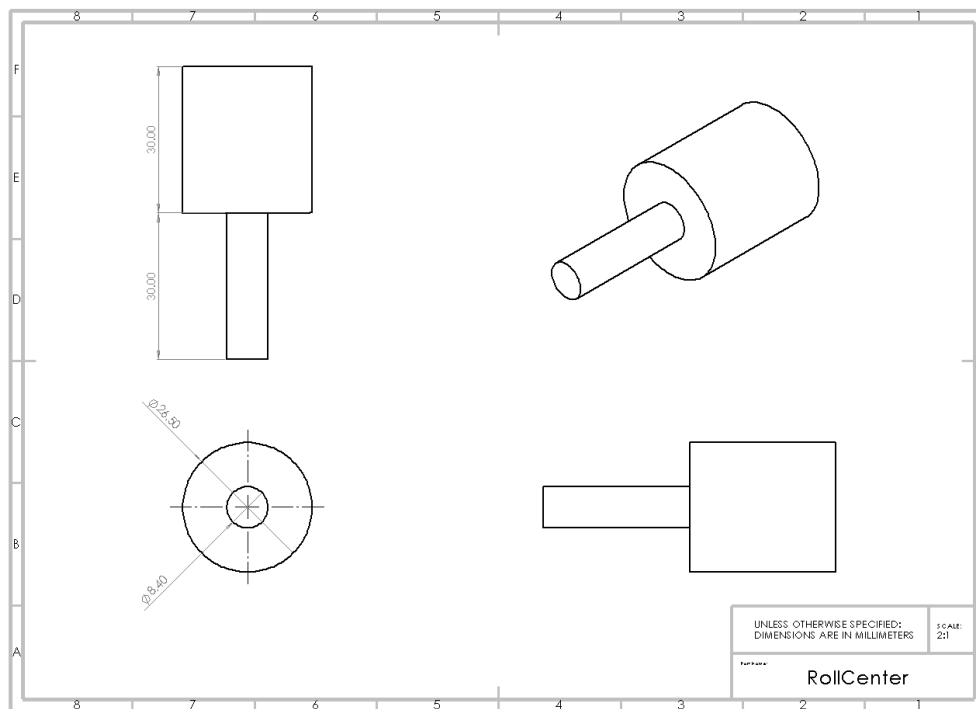


Figure 2: Rotating core dimensions.



## Automatic Experimental Set Up

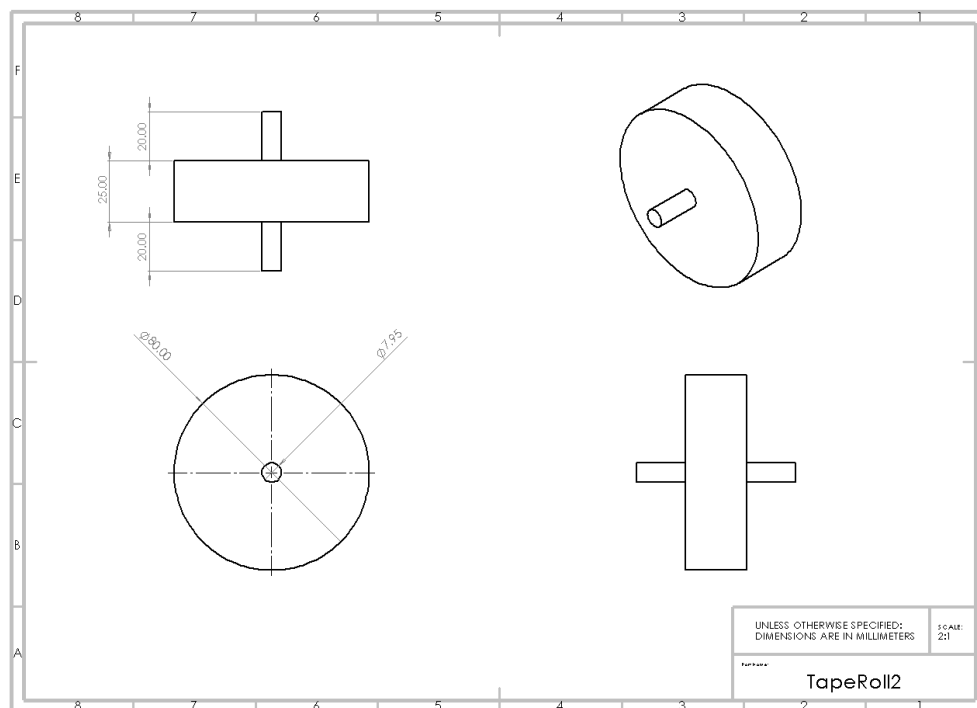


Figure 3: Tape spool dimensions.

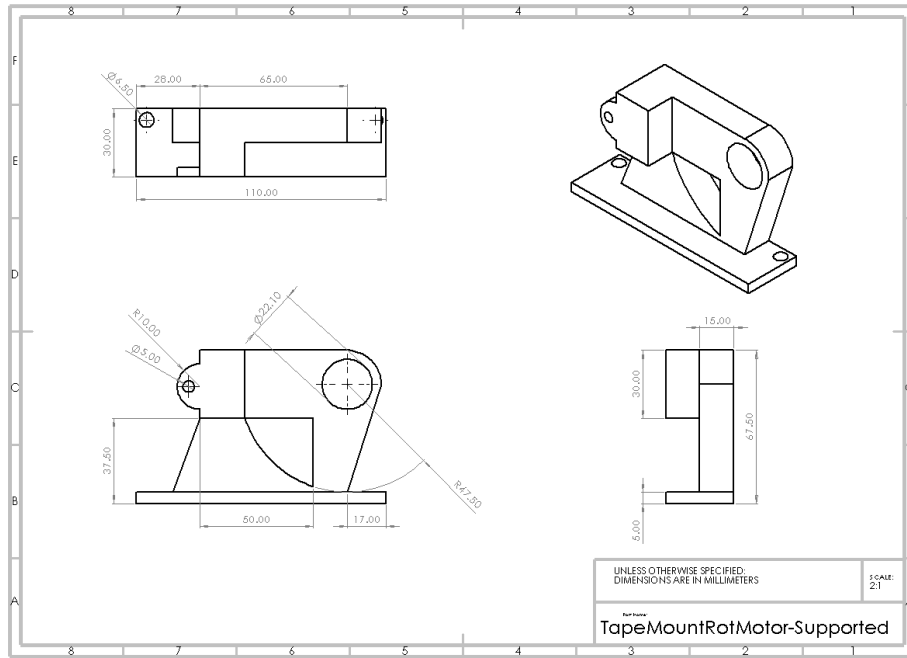


Figure 4: Supported mount half dimensions.

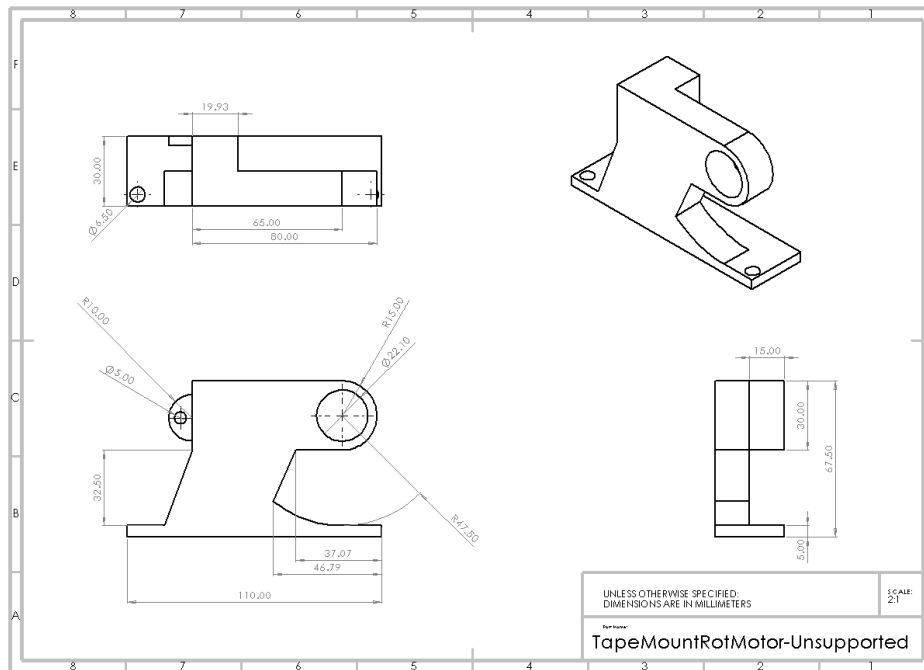


Figure 5: Unsupported mount half dimensions.

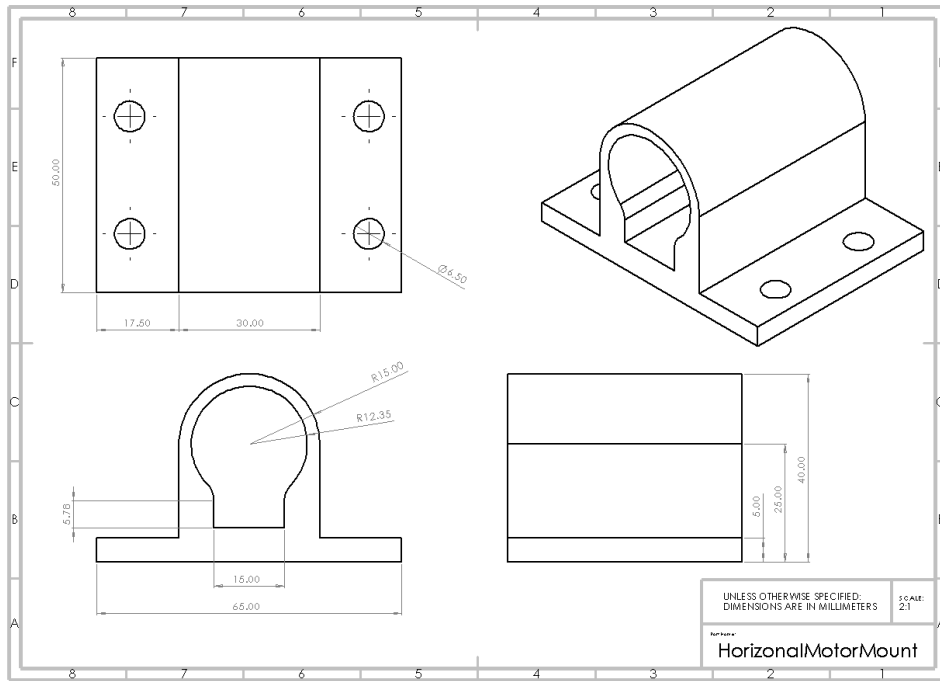


Figure 6: Motor mount dimensions.

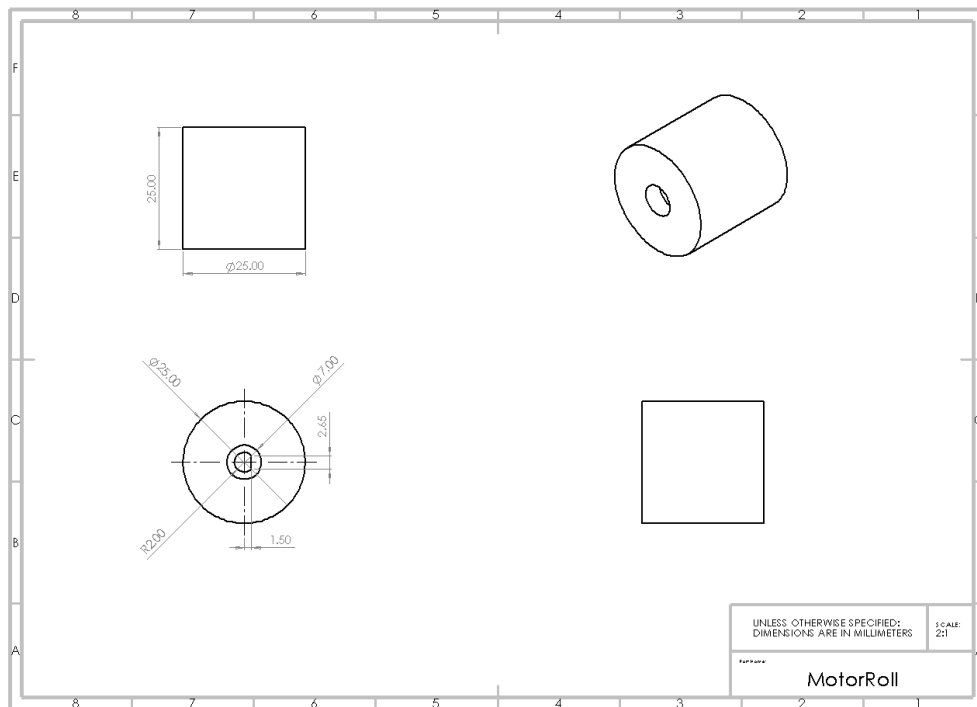


Figure 7: Motor pool dimensions.

## Appendix B Breadboard Configuration

This appendix presents the breadboard configuration used to power the Arduino and Bemonoc 12 V high speed DC gear motor. This breadboard configuration includes a TIP122 Darlington NPN Transistor, a blue LED, a 1 k $\Omega$  resistor between the transistor and the Arduino, and a 10 k $\Omega$  resistor between the LED and the transistor. This breadboard configuration was adapted from ME 454: Mechatronics Lab 7: DC Motors.

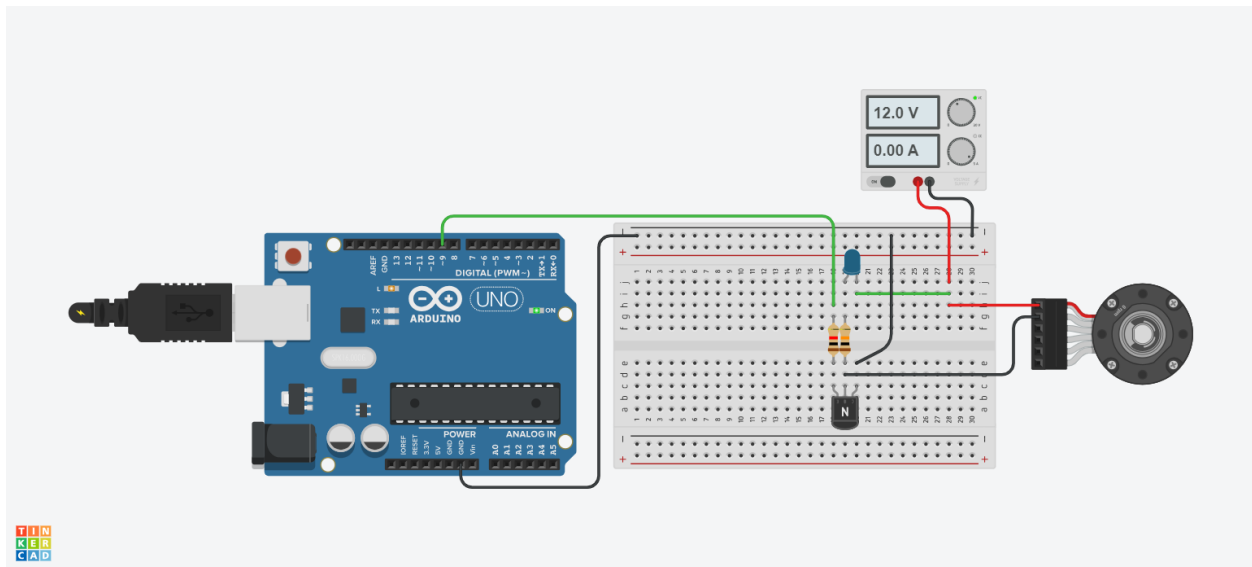


Figure 8: Breadboard configuration to interface motor and Arduino.

## Appendix C Arduino Code

This appendix presents the code uploaded to the Arduino to control the motor speed. This code can be modified to allow the motor to run at various rpm. This code was adapted from ME 454: Mechatronics Lab 7: DC Motors.

```
const byte motorPin = 9; // Define pin 9

void setup() {
  Serial.begin(9600); // Initialize
  pinMode(motorPin, OUTPUT); // sets the pin as output
}

void loop() {
  analogWrite(motorPin,250); // Writes the speed of the RPM
}
```